Nanocomposite Si/(NiTi) anode materials synthesized by high-energy mechanical milling for lithium-ion rechargeable batteries

Chadrasekhar Loka [a], HoTak Yu [a], Kee-Sun Lee [a,*], JongSoo Cho [b]

[a] Department of Advanced Materials Engineering, Kongju National University, Budaedong, Cheonan 330-717, South Korea
[b] Research Institute, MK electronics, Yongin 449-821, South Korea

HIGHLIGHTS

► Silicon and Nitinol powder mixture was milled by high-energy mechanical milling.
► High-energy mechanical milling results formation of nanocomposite Silicon/Nitinol.
► Coin cell cross sectional microstructure presented after cycling.
► Prominent electrochemical properties obtained due to nanocomposite structure.
► 10-h milled nanocomposite exhibit stable capacity of 553 mAh g^{-1} after 52nd cycle.

ARTICLE INFO

ABSTRACT

Nanocrystalline Silicon (Si) embedded Ni–Ti composite anode materials are synthesized by using two-stage high-energy mechanical milling (HEMM). The overall composition of the Si and NiTi (Nitinol) powders are 65 at.% and 35 at.%. The effects of crystal size, crystal structure, and microstructure on the electrochemical properties of the nanocomposite powders are examined through X-ray diffraction, scanning electron microscopy, high-resolution transmission electron microscopy, electrochemical test and nano-indentation test. The capacities of the coin cells produced with the 6 and 10 h milled powders are 711 and 553 mAh g^{-1}, respectively, after the 52nd cycle. The efficiencies of the coin cells produced with the 6 and 10 h milled powders continue to maintain 97.2 and 97.5%, respectively, until 52nd cycle. Coin cells produced with 10 h milled powders show relatively low capacity fading, which are attributed to the nanocomposite structure comprised of Si nanocrystals embedded into amorphous Ni–Ti matrix phase. Coin cell of 10 h milled powders reveals the reduced number of voids. Therefore, it is believed that Si embedded Ni–Ti nanocomposite using a two-stage high energy mechanical milling can be a promising candidate for high performance Si based anode materials.

© 2013 Elsevier B.V. All rights reserved.

1. Introduction

Lithium-ion rechargeable batteries have attracted more attention than other rechargeable batteries because of their superior performances such as higher energy density, higher operating voltages, and lower self-discharge, and because they are cost effective and safe [1–4]. Li-ion rechargeable batteries are widely used in the communications, electric vehicle (EV), and power storage sectors because these advantages can be readily exploited. Lithium easily reacts with several metals such as Sn, Sb, Al, Si, Pt, Ag, Zn, Cd, and Mg [5,6]. Among these metals, Si is the candidate with the most potential for application as an anode material

because of the high theoretical capacity of Si (Li$_{4.4}$Si: 4200 mAh g^{-1}) [4,7–11] and because it is inexpensive. Although Si is a potential candidate as an anode material, it unfortunately undergoes severe changes in volume (∼400%) during lithiation and delithiation, which results in pulverization of Si anode materials and leads to loss of electrical contact between the active material and current collector; hence, its capacity fading is severe [12–14]. Several Si-composite materials have been developed to solve these problems [15–22]. It has been reported that mechanical milling is effective to the formation of Si-nanocomposite structures, exhibiting excellent cyclability without severe cracking [23–26]. In the case of silicon as an electrochemically active material, higher capacities can be achieved while affording the utilization of the inactive matrix. Such a nanocomposite could allow for more efficient cyclability in a composite anode. This technology concept has been realized in systems such as Si/TiN, Si/TiB2, Si/SiC and Sn/C

* Corresponding author. Tel.: +82 41 521 9375; fax: +82 41 568 5776.
E-mail address: kslee@kongju.ac.kr (K.-S. Lee).

[27—29]. In particular, when the inactive phase was pre-milled and then again milled with Si, anodes made from the powder thus obtained showed better capacity retention than anodes containing a non-milled inactive phase [30], which was due to the smaller particle size of the inactive matrix, uniform distribution of stress throughout the electrode. However, in case that the matrix phase is exceedingly strong, Si crystals can be broken, which lead to the serious capacity fading. Therefore, it is necessary to find out the inactive matrix materials with ability to compensate the stress induced by Si volume expansion. Currently, some researchers has been tried to utilize super-elastic Nickel—Titanium (NiTi) alloy (nitinol) [31] as inactive matrix phase by using various methods such as melt-spinning and thin film deposition [32—34]. They expected that the super-elastic matrix could accommodate the stress driven by Si volume changes during charging and discharging. In present work, we investigate the possibility that Si embedded nanocomposite structure (Si/NiTi) can be synthesized by using high energy mechanical milling (HEMM) process, which is favorable to large scale production [23,24]. At first we prepared submicrometer sized Si powders from the first stage of mechanical milling and then the active Si is milled with NiTi alloy powders produced by gas atomization (in second stage-HEMM).

This study covers the crystal structure changes and Si distribution in Ni—Ti matrix and their electrochemical properties.

2. Experimental

2.1. Material preparation

Si/(NiTi) nanocomposite powder was prepared using a Simoloyer CM01 (Zoz GmbH, Germany) HEMM system, which was controlled using MALTOZ-software. The nanocomposite powder was prepared in two steps: (1) Commercially obtained Si powder (average particle size: <40 μm, 98% purity) was milled for 12 h; (2) the milled Si powder from step (1) was mixed with NiTi alloy powder produced by gas atomization (average particle size: <60 μm, 99% purity) in a ratio of 65 at.% Si and 35 at.% NiTi. This mixture is termed "as-mixed powder". Samples of the as-mixed powder were milled for either 6 or 10 h to form two Si/(NiTi) nanocomposite phases. The entire milling process was performed at room temperature in a firmly sealed hardened vial and under a completely inert ambient atmosphere to eliminate oxidation. Yttrium-stabilized zirconia (YSZ) balls were used as the milling media, and the ball-to-powder weight ratio was maintained at 30:1. Stearic acid (5 wt%) was used as a process controlling agent (PCA), and the rotation speed of impeller was 800 rpm.

2.2. Characterization of materials

Phase analysis was performed using X-ray diffraction (XRD) with Cu-K$_\alpha$ radiation ($\lambda = 1.5418$ A) operating at 8 kW and step size is 0.02° from 20 to 80° in the 2θ range. Field-emission scanning electron microscopy (FE-SEM) and high-resolution transmission electron microscopy (HR-TEM) were used to observe cross-sections of the milled powders and the coin cells produced with them. In particular, the cross-section of the coin cell was prepared by ion-milling after the extraction of Li-ion, and the anode plate was taken out in the glove box filled with Ar gas. To compare mechanical behavior between Si and Si/(Ni—Ti), nano-indentation test (Fischer, HM2000XYP) for obtaining hardness, elastic modulus and elastic strain were performed. Vickers diamond indenter was employed. The modulus and hardness was measured at load of 30 mN. All the obtained data were calibrated using a fused silica reference. For the preparation of test specimen, Si/(Ni—Ti) powders were mixed with acrylic powder and then pressed at 200 °C and

then cooled to room temperature. The test specimen was shown in the schematic diagram Fig. 1.

2.3. Electrochemical tests

For the electrochemical evaluation, the milled Si/(NiTi) electrodes were prepared by coating Cu substrates with a slurry containing the following materials dissolved in N-methyl-2-pyrrolidinone (NMP): the active material (80 wt%), SFG6 graphite (10 wt%), Ketjenblack® (2 wt%) as a conductive agent, and polyamide-imide (PAI, 8 wt%) as a binder material. The electrodes were pressed and dried under vacuum at 350 °C for 1 h. They were then cut into 14-mm-diameter discs. Coin-type electrochemical cells were assembled in an Ar-filled glove box. Celgard® 2400 was used as the separator, Li foil was used as both the counter and reference electrodes, and a 1-M solution of LiPF$_6$ (lithium hexafluorophosphate) dissolved in a mixture of ethylene carbonate (EC)/diethyl carbonate (DEC)/fluoroethylene carbonate (FEC) (5:70:25 by volume) was used as the electrolyte. Charge/discharge measurements (TOSCAT-3100, Toyo System Co., Ltd.) for the composite anodes were performed when constant current (CC) is applied over a voltage range of 0.01 and 1.5 V (constant current density of 2.5 mA cm^{-2}) at 0.1 and 0.2 C-rate for first and second cycles respectively, and 1.0 C-rate from third cycle.

3. Results and discussion

3.1. Evolution of composite structures

X-ray diffraction patterns for the pure Si, pure NiTi, and Si/(NiTi) composite powders are presented in Fig. 2. The intensities of the Si diffraction peaks (Fig. 2(a)) reduce with increasing milling time, which indicates pulverization of the Si powders during mechanical milling. The diffraction pattern for pure NiTi powder is presented in Fig. 2(b). The diffraction patterns for the Si/(NiTi) composite powders obtained after various milling times are shown in Fig. 2(c). In the 6 h milled composite powders, the peaks inside the rings indicate that the crystalline NiTi phase transforms into the nanocrystalline and amorphous phase. In particular, the 10 h milled composite powders, the amorphization is continued to proceed. Accordingly, the Si diffraction peaks are not changed significantly with increasing milling time and instead NiTi (Nitinol) peaks are abruptly broaden and their intensities are decreased, which indicates the phase transition from crystalline NiTi to (nanocrystalline + amorphous) Ni—Ti. From the XRD results, no significant contamination relevant peaks were observed due to YSZ balls (milling media) and PCA.
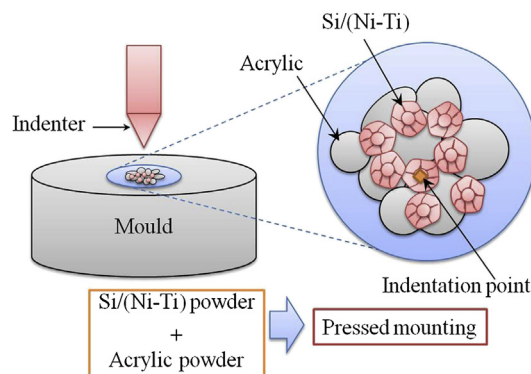

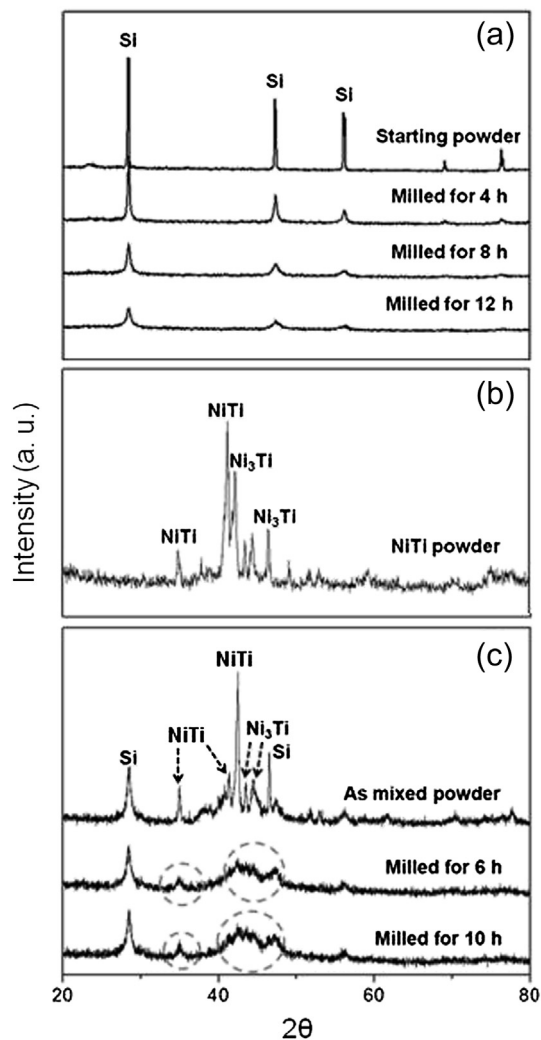Fig. 1. Schematic illustration for preparation of Si/(Ni—Ti) nano-indentation test specimen.

Fig. 2. XRD patterns obtained from powders milled for various milling times. (a) Pure Si powder (step (1)), (b) pure NiTi powder and (c) Si/(NiTi) composite powder (step (2)).

Fig. 3. Cross-sectional SEM images of Si/(NiTi) composite powders milled for (a) 6 h and (b) 10 h.

As shown in cross-sectional SEM (back scattered electron) images (Fig. 3), composite structures mixed with Si and NiTi powders are obtained. The black and gray regions are distinguished as Si and NiTi phases, respectively. A more random distribution of phases is obtained in the 10 h milled powders than in the 6 h milled powders.

TEM (and HR-TEM) analysis are performed for the composite powders, as shown in Fig. 4. The gray and black irregular shaped phases in the 6 h milled powders (Fig. 4(a)) are observed, which are identified as nanocrystalline Si and NiTi phases respectively from the ring patterns of points P-1 and P-2 (inserted in the micrograph). In addition, the high-resolution image (Fig. 4(b)), reveals inter planar distance of nanocrystals, which confirms Si (0.32 nm) and NiTi (0.21 nm) by comparing to the theoretical values (0.312 and 0.214 nm, respectively) from the Joint Committee for Powder Diffraction Standards (JCPDS) data. Consequently, it is difficult to obtain homogeneous nanocomposite structures comprised of nano-Si and NiTi phases in the 6 h milled powders. Fig. 4(c) shows the micrograph of the 10 h milled powders. Comparing to 6 h milled powders, relatively homogeneous structures are obtained, in which nanosized Si crystals seem to be embedded into the Ni–Ti phase. From diffraction spots and diffused ring pattern which is inserted in Fig. 4(c), it is expected that most of the phases in 10 h
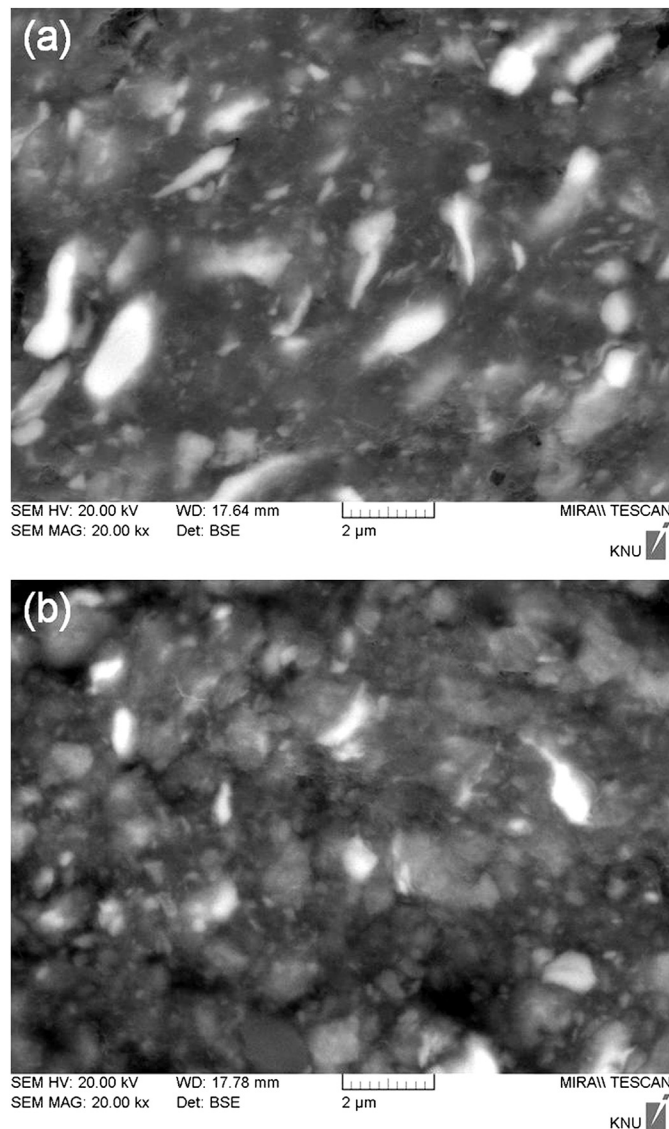
milled powders are comprised of nanocrystalline and amorphous phases. In particular, the high-resolution image (Fig. 4(d)) evidently shows that most of the phases are comprised of amorphous Ni–Ti phase including nanocrystalline Si and small amount of NiTi phases, which is consistent with the XRD results. Initially NiTi powder comprised of intermetallic phase would be severely deformed depending on milling time. Depending on milling time, the intermetallic compound can be transformed into nanocrystalline and amorphous phase [35,36].

3.2. Electrochemical performance

The electrochemical characteristics of coin cell obtained with the 6 and 10 h milled composite powders are evaluated, charging (lithiation) and discharging (delithiation) curves of 6 and 10 h milled powders are shown in Fig. 5(a) and (b) respectively. Voltage profiles of both powders are similar. The charging curves in both 6 and 10 h powders are overlapped except first cycle. In particular, 10 h milled powders exhibit no significant changes with respect to cycle number in discharging curves except for first cycle. In
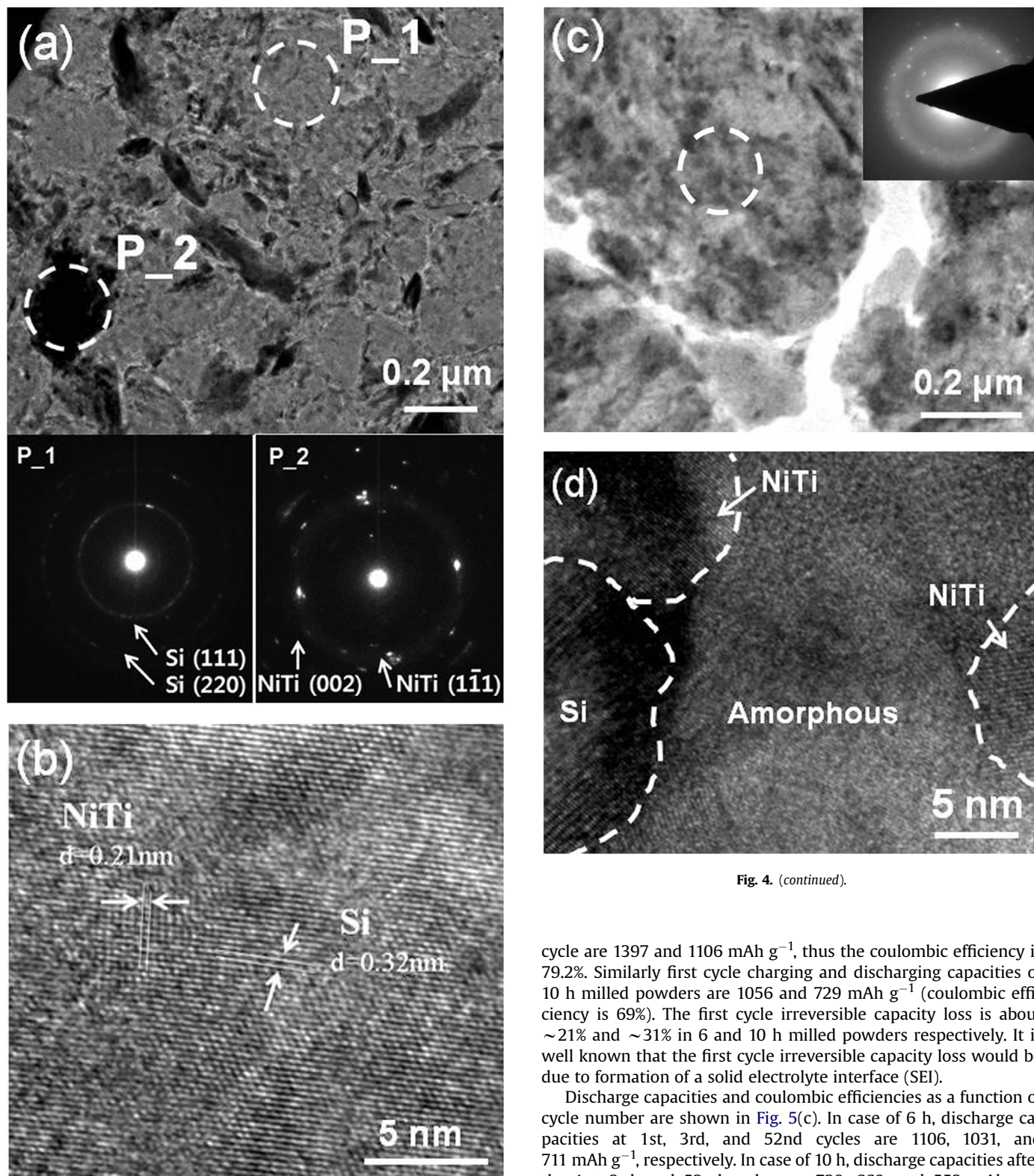
Fig. 4. (HR) TEM images and ring patterns for Si/(NiTi) nanocomposite powders milled for 6 h (a, b) and 10 h (c, d).

addition, we can observe a shift in discharge potential plateau from the first cycle to the third cycle in both 6 and 10 h milled powders, which could be related to the silicon phase transformation from the crystalline to the amorphous during the first discharge [37–40]. In 6 h milled powders, the charging and discharging capacities of first

Fig. 4. (continued).

cycle are 1397 and 1106 mAh g^{-1}, thus the coulombic efficiency is 79.2%. Similarly first cycle charging and discharging capacities of 10 h milled powders are 1056 and 729 mAh g^{-1} (coulombic efficiency is 69%). The first cycle irreversible capacity loss is about ~21% and ~31% in 6 and 10 h milled powders respectively. It is well known that the first cycle irreversible capacity loss would be due to formation of a solid electrolyte interface (SEI).

Discharge capacities and coulombic efficiencies as a function of cycle number are shown in Fig. 5(c). In case of 6 h, discharge capacities at 1st, 3rd, and 52nd cycles are 1106, 1031, and 711 mAh g^{-1}, respectively. In case of 10 h, discharge capacities after the 1st, 3rd, and 52nd cycles are 729, 669, and 553 mAh g^{-1}, respectively. Longer milling time reduces initial capacity and enhances the capacity retention (cyclic stability). The first cycle coulombic efficiencies (C/D efficiencies) for 6 and 10 h milled powders are 79.2% and 69% respectively. The C/D efficiencies abruptly increase until the 10th cycle and are saturated to 97.2 (6 h) and 97.5% (10 h), respectively. In spite of the capacity difference depending on milling time, no noteworthy difference in the efficiency is observed.
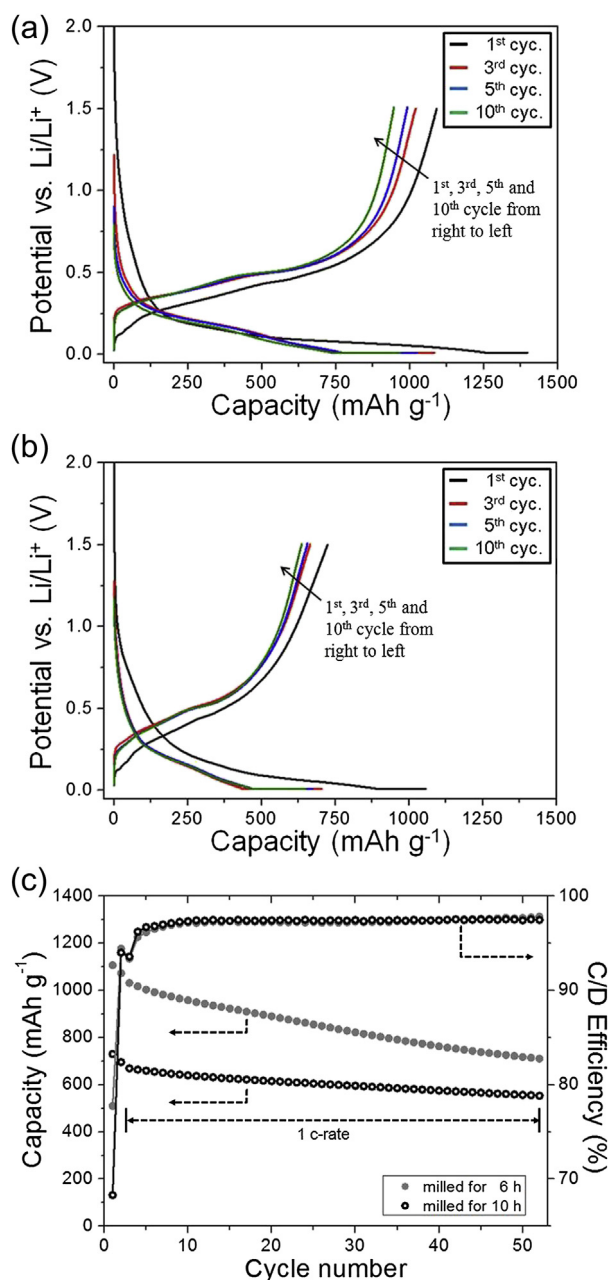
on TEM micrograph, Si crystals are smaller in 10 h milled powders. Moreover, it has been reported that smaller particles can reduce the electronic and ionic transport distances and decrease the stress induced by inhomogeneous Li diffusion [28,41]. Therefore, 10 h milled powders are satisfied with two factors for enhancement of capacity retention; homogeneous nanocomposite structure and active Si crystal size effect.

In order to elucidate the enhanced capacity retention during lithiation and delithiation, the cross sections of coin cells are observed as shown in Fig. 6. The cross section of coin cell (25th cycle) with 6 h milled powders exhibits significant number of nanovoids and the voids are larger. In case of 10 h, nanovoids in the coin cell (52nd cycle) are relatively lesser and smaller in size. The finding of nanovoids in the coin cell cross section has rarely been
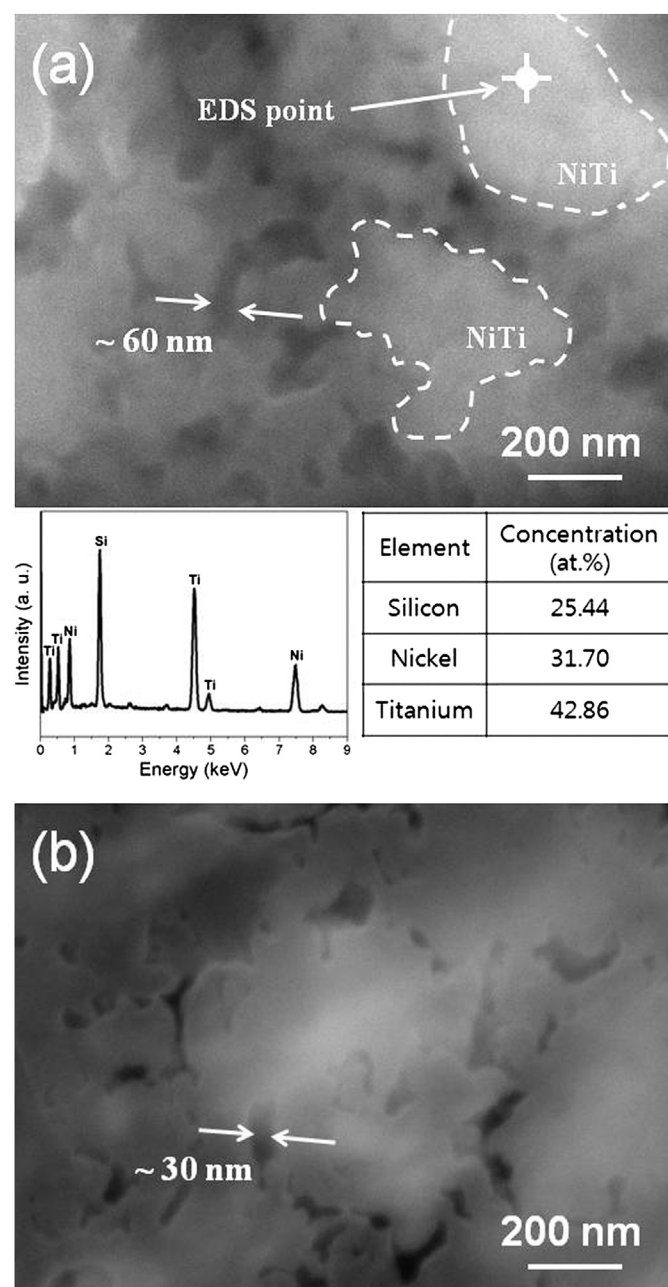
Fig. 5. Charging/discharging curves and cycling performances of Si/(NiTi) nano-composite powders milled for 6 h and 10 h; (a, b) charging/discharging curves and (c) discharge capacity and coulombic efficiency as a function of cycle number.

It has been reported that the Si crystals can be encompassed by inactive and less active phases with increasing milling time, leading to the reduced phase fraction of the active Si and degraded initial capacity [27,28,30]. As discussed in the XRD results (Fig. 2(c)) and (HR) TEM images (Fig. 4), nanocrystalline Si are isolated by inactive Ni–Ti phase. Consequently, the reduced initial capacities are believed to be due to not only SEI formation but also the active Si encompassed by inactive Ni–Ti phase.

Capacity retention in case of 10 h is prominent comparing to that of 6 h, which is expected to be related with nanocomposite structure comprised of Si and Ni–Ti phase. Longer milling is desirable to provide random distribution of constituent phases as shown in SEM (Fig. 3) and TEM (Fig. 4) images. In addition, the capacity retention is closely related with active Si crystal size. Based

Fig. 6. Cross-sectional SEM images and EDS spectrum of coin cell obtained at specific milling time and cycle conditions. (a) 6 h − 25th cycle and (b) 10 h − 52nd cycle.

reported. The energy-dispersive X-ray spectroscopy (EDS) point analysis indicates that the white region in the 6 h milled composite powder is the NiTi phase (the corresponding EDS spectrum is shown in Fig. 6(a)). Hence, the gray region is the active-Si phase. The nanovoids are obviously only observed in active phase, not in inactive phase, irrespective of milling time. In particular, nanovoids tend to initiate at active-inactive phase boundaries and continue to propagate toward active Si phase, which indicates lithium-ion can diffuse in and out by way of active Si/(Ni−Ti) matrix interface. Based on the cross sectional micrographs of coin cells, it is believed that the formation of nanovoids is due to volume changes difference between Si and matrix phase during lithium-ion extraction. As discussed in the SEM and HR-TEM analysis, the distribution of Si nanocrystals and Ni−Ti phase becomes more random with increasing milling time. Since the Si particles are large and the distribution of both the Si and NiTi phases are relatively inhomogeneous in the 6 h milled powder, a significant number of nanovoids can form during lithiation and delithiation despite the effect of the super-elastic NiTi matrix. Hence, fewer nanovoids are observed in the 10 h milled powder (Fig. 6(b)) compare to 6 h milled powder. In addition, we suppose that the smaller Si crystals can reduce the magnitude of the stress and strain concentration at the interface of Si/(Ni−Ti) during lithiation and delithiation. This result suggests that smaller Si crystals embedded into nanocomposite structures are effective in reducing volume changes during lithiation and the nanovoids can affect electrochemical properties. In view of nanovoid formation, it is reasonable that at least 10 h mechanical milling is necessary in order to restrain the number and size of nanovoids during cycling.

Differential capacity plots (DCPs) corresponding to the coin cells of Si/(NiTi) nanocomposites of 6 and 10 h milled powders are shown in Fig. 7. Pure Si shows two peaks at 0.38 V and 0.56 V
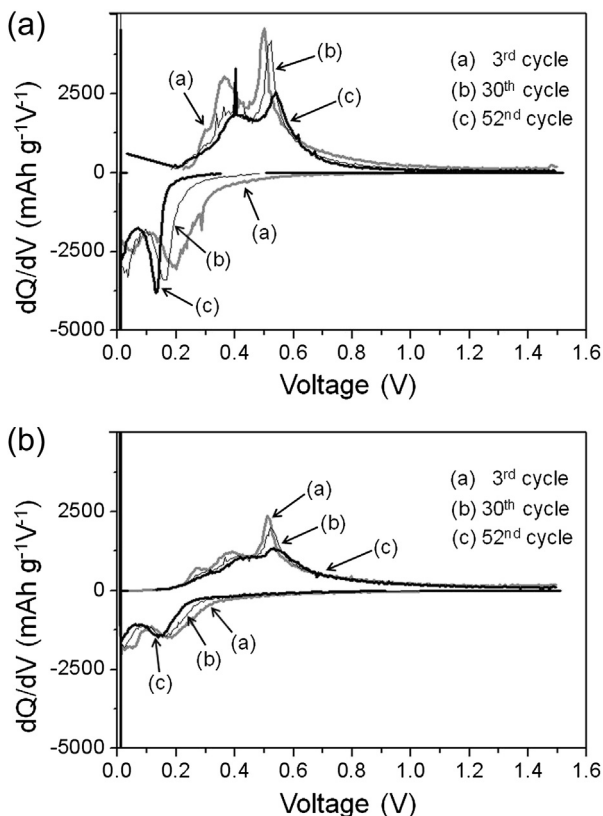

Fig. 8. Loading and unloading curves of Si wafer and Si/(Ni−Ti) obtained from nano-indentation test at a loading rate of 1.5 mN s^{-1}.

[17,42,43], which are in accordance with the values of 0.36 V and 0.5 V in coin cells produced by 6 and 10 h milling, indicating de-alloying during discharging in the third cycle. During charging, the peak observed at 0.24 and 0.28 V indicates the alloying of Li$^+$ with Si below 0.3 V [44]. After the 30th and 52nd cycles, the peaks slightly shift and broaden. In particular, the peaks are seriously broaden in 10 h milled powders. Since the broadened peaks attribute to the conversion of crystalline Si to amorphous Li−Si phase during lithiation [45,46], smaller Si crystals are desirable to obtain enhanced capacity retention.

3.3. Nano-indentation test

Fig. 8 shows the nano-indentation test results for Si wafer (Si wafer is assumed as active Si) and Si/(Ni−Ti) (milled for 10 h). Hardness and elastic modulus of Si and Si/(Ni−Ti) are 7.9, 77.4 GPa and 2.9, 18.4 GPa, respectively. Elastic strain range of Si/(Ni−Ti) is significantly larger compared to Si. For example, the indentation depth of the Si is ∼460 nm at 30 mN of the load and then is recovered to ∼244 nm at unloaded (0 mN) state. However the indentation depth of Si/(Ni−Ti) is ∼896 nm at the same load and recovered to ∼337 nm at unloaded state. In addition, considering the area (defined by dashed lines in Fig. 8), recoverable energy (elastic strain energy) of Si/(Ni−Ti) is approximately 2.58 times higher than that of Si at the same loading and unloading conditions. This result indicates that (Ni−Ti) composite phase has the capability to accommodate elastically the stress generated by Si expansion during lithiation. After 10 h milling we obtained Ni−Ti amorphous matrix instead of crystalline NiTi (Nitinol) matrix. Despite, the Ni−Ti amorphous matrix shows significant elastic characteristics. Consequently, we have succeeded highly elastic nanocomposite structure comprised of the amorphous Ni−Ti matrix and randomly dispersed Si nanocrystals.

We can deduce that the factors ascribed to stable capacity are the presence of nanocrystalline Si, an effective amorphous Ni−Ti matrix which has high elastic nature (which can act as a buffer to accommodate the changes in Si volume during lithiation and delithiation), limited number of nanovoids, and randomly distributed nanocomposite structures.

4. Conclusions

In this study, nanocomposite Si/(Ni−Ti) powders comprised of active Si crystals embedded into an inactive Ni−Ti matrix phase

Fig. 7. Differential capacity plots (DCPs) of 3rd, 30th, and 52nd cycles for coin cells produced with (a) 6 h and (b) 10 h milled Si/(NiTi) nanocomposite powders.
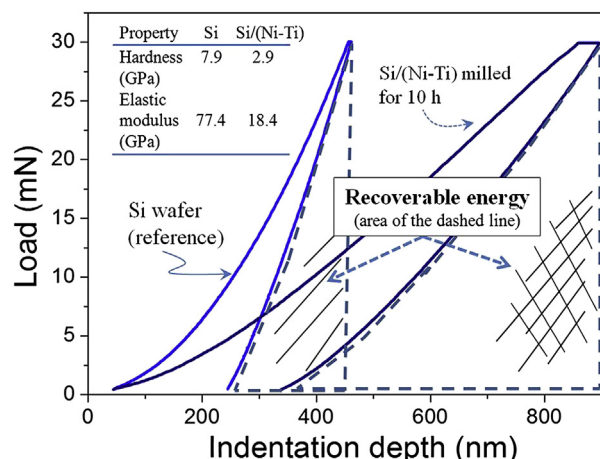
were produced using a two-stage HEMM. Discharge capacity profiles revealed that the coin cell produced with the 10 h milled composite powder exhibited a cycling capacity of about 553 mAh g^{-1} after the 52nd cycle and better capacity retention than the coin cycle produced with the 6 h milled powder. The coulombic efficiencies after 10th cycle were 97.2 and 97.5% for the coin cells produced with the 6 and 10 h milled powders, respectively. The initial capacity decreases with increasing milling time because of the formation of SEI and encompassment of active Si by the Ni–Ti phase. The cross-sectional images of the coin cells revealed nanovoids, which are closely related with capacity retention and changes in Si volume during lithiation and delithiation. Fewer nanovoids existed in the 10 h milled powders than in the 6 h milled powders, which indicated the presence of Si nanocrystals and the effective distribution of the Si nanocrystals throughout the amorphous Ni–Ti matrix. Therefore, it is believed that the prominent electrochemical properties of the nanocomposite Si/(Ni–Ti) powders are attributed to the nanocomposite structure comprised of Si nanocrystals and the buffering of the amorphous Ni–Ti phase. These results suggest that the Si/(Ni–Ti) nanocomposite is a very promising system for lithium-ion anode material in view of high capacity and stable cycle performance.

Acknowledgments

References

[1] J.M. Tarascon, M. Armand, Nature 414 (2001) 359–367.
[2] G.X. Wang, L. Sun, D.H. Bradhurst, S. Zhong, S.X. Dou, H.K. Liu, J. Power Sources 88 (2000) 278–281.
[3] R.A. Huggins, J. Power Sources 26 (1989) 109–120.
[4] W.J. Weydanz, M. Wohlfahrt, R.A. Huggins, J. Power Sources 81 (1999) 237–242.
[5] M. Winter, J.O. Besenhard, Electrochim. Acta 45 (1999) 31–50.
[6] W.J. Zhang, J. Power Sources 196 (2011) 13–24.
[7] U. Kasavajjula, C. Wang, A.J. Appleby, J. Power Sources 163 (2007) 1003–1039.
[8] J.O. Besenhard, J. Yang, M. Winter, J. Power Sources 68 (1997) 87.
[9] N. Ding, J. Xu, Y. Yao, G. Wegner, I. Lieberwirth, C. Chena, J. Power Sources 192 (2009) 644.
[10] J.C. Arrebola, A. Caballero, J.L.G. Camer, L. Hernen, J. Morales, L. Sanchez, Electrochem. Commun. 11 (2009) 1061.
[11] Q. Si, K. Hanai, N. Imanishi, M. Kubo, A. Hirano, Y. Takeda, O. Yamamoto, J. Power Sources 189 (2009) 761–765.
[12] Z. Edfouf, F. Cuevas, M. Latroche, C. Georges, C. Jordy, T. Hezeque, G. Caillon, J.C. Jumas, M.T. Sougrati, J. Power Sources 196 (2011) 4762–4768.
[13] R. Benedek, M.M. Thackeray, J. Power Sources 110 (2002) 406.
[14] K. Li, X. Huang, L. Chen, Z. Wu, Y. Liang, Electrochem. Solid-State Lett. 2 (1999) 547.
[15] J.-H. Kim, H. Kim, H.-J. Sohn, Electrochem. Commun. 7 (2005) 557.
[16] S. Yoon, S.-I. Lee, H. Kim, H.-J. Sohn, J. Power Sources 161 (2006) 1319.
[17] M.-S. Park, Y.-J. Lee, S. Rajendran, M.-S. Song, H.-S. Kim, J.-Y. Lee, Electrochim. Acta 50 (2005) 5561.
[18] H.-Y. Lee, S.-M. Lee, Electrochem. Commun. 6 (2004) 465.
[19] Y. Liu, K. Hanai, J. Yang, N. Imanishi, A. Hirano, Y. Takeda, Electrochem. Solid-State Lett. 7 (2004) A369.
[20] Y. Liu, K.T. Matsumura, N. Imanishi, A. Hirano, T. Ichikawa, Y. Takeda, Electrochem. Solid-State Lett. 8 (2005) A599.
[21] J. Yang, B.F. Wang, K. Wang, Y. Liu, J.Y. Xie, Z.S. Wen, Electrochem. Solid-State Lett. 6 (2003) A154.
[22] M. Yoshio, H. Wang, K. Fukuda, T. Umeno, N. Dimov, Z. Ogumi, J. Electrochem. Soc. 149 (2002) A1598.
[23] O. Mao, R.L. Turner, I.A. Courtney, B.D. Fredericksen, M.I. Buckett, L.J. Krause, J.R. Dahn, Electrochem. Solid-State Lett. 2 (1999) 3.
[24] P. Patel, I.-S. Kim, P.N. Kumta, Mater. Sci. Eng. B 116 (2005) 347–352.
[25] M. Yoshio, S. Kungino, N. Dimov, J. Power Sources 153 (2006) 375–379.
[26] C.K. Chan, H. Peng, G. Liu, K. Mcilwrath, X.F. Zhang, R.A. Huggins, Y. Cui, Nat. Nanotechnol. 3 (2008) 31.
[27] I. Kim, P.N. Kumta, G.E. Blomgren, Electrochem. Solid-State Lett. 3 (2000) 493.
[28] I. Kim, G.E. Blomgren, P.N. Kumta, Electrochem. Solid-State Lett. 6 (2003) A157.
[29] I. Kim, G.E. Blomgren, P.N. Kumta, Proc. Electrochem. Soc. 36 (2001) 185–196.
[30] Z.P. Guo, Z.W. Zhao, H.K. Liu, S.X. Dou, J. Power Sources 146 (2005) 190–194.
[31] K. Otsuka, X. Ren, Prog. Mater. Sci. 50 (2005) 511.
[32] S.-B. Son, S.C. Kim, C.S. Kang, T.A. Yersak, Y.-C. Kim, C.-G. Lee, S.-H. Moon, J.S. Cho, J.-T. Moon, K.H. Oh, S.-H. Lee, Adv. Energy Mater. 2 (2012) 1226–1231.
[33] H. Jung, Y.-U. Kim, M.-S. Sung, Y. Hwa, G. Jeong, G.-B. Kim, H.-J. Sohn, J. Mater. Chem. 21 (2011) 11213–11216.
[34] R. Hu, M. Zhu, H. Wang, J. Liu, O. Liuzhang, J. Zou, Acta Mater. 60 (2012) 4695–4703.
[35] D.-Z. Sun, L.-Z. Cheng, Y.-M. Zhang, K.-Y. Ho, J. Alloys Compd. 186 (1992) 33–35.
[36] C. Suryanarayana, Prog. Mater. Sci 46 (2001) 1–184.
[37] K. Hanai, Y. Liu, N. Imanishi, A. Hirano, M. Matsumura, T. Ichikawa, Y. Takeda, Electrochem. Commun. 5 (2003) 165–168.
[38] L.Y. Beaulieu, T.D. Hachard, A. Bonakdarpour, M.D. Fleischauer, J.R. Dahn, J. Electrochem. Soc. 150 (2003) A1457.
[39] M.N. Obrovac, L. Christensen, Electrochem. Solid-State Lett. 7 (2004) A93.
[40] T.D. Hatchard, J.R. Dahn, J. Electrochem. Soc. 151 (2004) A838.
[41] A.D.W. Todd, P.P. Ferguson, J.G. Barker, M.D. Fleischauer, J.R. Dahn, J. Electrochem. Soc. 156 (2009) A1034.
[42] K.-M. Lee, Y.-S. Lee, Y.-W. Kim, Y.-K. Sun, S.-M. Lee, J. Alloys Compd 472 (2009) 461.
[43] I. Kim, G.E. Blomgren, P.N. Kumta, J. Power Sources 130 (2004) 275–280.
[44] W. Wang, P.N. Kumta, J. Power Sources 172 (2007) 650–658.
[45] J.-B. Kim, S.-H. Lim, S.-M. Lee, J. Electrochem. Soc. 153 (2006) A455.
[46] H. Li, X. Huang, L. Chen, G. Zhou, Z. Zhang, D. Yu, Y.J. Mo, N. Pei, Solid State Ionics 135 (2000) 181–191.